Journal of Rock Mechanics and Geotechnical Engineering 15 (2023) 1127–1143

Contents lists available at ScienceDirect

Journal of Rock Mechanics and Geotechnical Engineering

journal homepage: www.jrmge.cn

Full Length Article

Landslide susceptibility prediction using slope unit-based machine learning models considering the heterogeneity of conditioning factors

Zhilu Chang [a,b], Filippo Catani [b], Faming Huang [a,*], Gengzhe Liu [c], Sansar Raj Meena [b], Jinsong Huang [a,d], Chuangbing Zhou [a]

[a] School of Infrastructure Engineering, Nanchang University, Nanchang, 330031, China
[b] Department of Geosciences, University of Padova, Padova, Italy
[c] School of Design, University of Pennsylvania, Philadelphia, PA, 19104, USA
[d] Discipline of Civil, Surveying and Environmental Engineering, College of Engineering, Science and Environment, The University of Newcastle, Callaghan, NSW, 2308, Australia

ARTICLE INFO

Article history:
Received 18 March 2022
Received in revised form
7 June 2022
Accepted 17 July 2022
Available online 11 August 2022

Keywords:
Landslide susceptibility prediction (LSP)
Slope unit
Multi-scale segmentation method (MSS)
Heterogeneity of conditioning factors
Machine learning models

ABSTRACT

To perform landslide susceptibility prediction (LSP), it is important to select appropriate mapping unit and landslide-related conditioning factors. The efficient and automatic multi-scale segmentation (MSS) method proposed by the authors promotes the application of slope units. However, LSP modeling based on these slope units has not been performed. Moreover, the heterogeneity of conditioning factors in slope units is neglected, leading to incomplete input variables of LSP modeling. In this study, the slope units extracted by the MSS method are used to construct LSP modeling, and the heterogeneity of conditioning factors is represented by the internal variations of conditioning factors within slope unit using the descriptive statistics features of mean, standard deviation and range. Thus, slope units-based machine learning models considering internal variations of conditioning factors (variant slope-machine learning) are proposed. The Chongyi County is selected as the case study and is divided into 53,055 slope units. Fifteen original slope unit-based conditioning factors are expanded to 38 slope unit-based conditioning factors through considering their internal variations. Random forest (RF) and multi-layer perceptron (MLP) machine learning models are used to construct variant Slope-RF and Slope-MLP models. Meanwhile, the Slope-RF and Slope-MLP models without considering the internal variations of conditioning factors, and conventional grid units-based machine learning (Grid-RF and MLP) models are built for comparisons through the LSP performance assessments. Results show that the variant Slope-machine learning models have higher LSP performances than Slope-machine learning models; LSP results of variant Slope-machine learning models have stronger directivity and practical application than Grid-machine learning models. It is concluded that slope units extracted by MSS method can be appropriate for LSP modeling, and the heterogeneity of conditioning factors within slope units can more comprehensively reflect the relationships between conditioning factors and landslides. The research results have important reference significance for land use and landslide prevention.

1. Introduction

Landslides are a widespread geological disaster globally, causing thousands of deaths and billions of property loss (Hungr et al., 2013; Chen et al., 2022; Zhang et al., 2022a, b, c). It is necessary to predict the spatial distribution of potential landslides, which plays an important role in the policy of land use, physical and ecological environment protection. However, how to accurately predict the potential locations of future potential landslides remains a great challenge (Alcántara-Ayala et al., 2017). The landslide susceptibility prediction (LSP) can effectively resolve this issue based on the recorded landslide inventory and related conditioning factors (Reichenbach et al., 2018).

LSP modeling is generally constructed on the basis of the characteristics of recorded landslides and landslide-related

* Corresponding author.
E-mail address: huang1503518@sina.cn (F. Huang).
Peer review under responsibility of Institute of Rock and Soil Mechanics, Chinese Academy of Sciences.

https://doi.org/10.1016/j.jrmge.2022.07.009

conditioning factors (Chen et al., 2015; Huang et al., 2017). Then, the landslide susceptibility indices (LSIs) or mappings (LSMs) are obtained through: collecting base maps of recorded landslides and geo-environmental factors; extracting appropriate mapping unit; obtaining landslide-related conditioning factors; constructing LSP models; calculating LSIs and producing LSMs (Guzzetti et al., 2005; Samia et al., 2018). Among these processes, it is revealed that the selections of mapping unit, conditioning factors and LSP models have significant effects on the LSP results (Ba et al., 2018; Reichenbach et al., 2018; Tang et al., 2020). In the past 20 years, most researchers have mainly concentrated on the comparison of LSP results from the perspective of LSP models and their performance assessment (Park et al., 2018; Sur et al., 2020). However, the effects of different mapping units and conditioning factors on LSP modeling have not been explored in depth, leading to some biases between LSMs and spatial distribution of field actual landslides.

The issue of appropriate mapping unit selection is an important pre-requisite to obtain more accurate and reasonable LSP results (Guzzetti et al., 1999). Literature review shows that the grid unit and the slope unit are two commonly used mapping units, while the unique condition unit and small watershed unit are rarely used (Huang et al., 2020; Jacobs et al., 2020). The grid unit is the most common mapping unit due to the simple mathematical modeling and computation of LSP in different geographical regions (Reichenbach et al., 2018). However, there is no direct physical relation between grid units and the geomorphological information connected to landslides. Moreover, the LSP results based on the grid units may generate some weaknesses in practical application because the potential landslide boundary is difficult to accurately determine. In contrast, slope units can perfectly overcome those drawbacks existing in the grid units, resulting in more attempts for LSP modeling using slope units in recent researches (Domènech et al., 2019; Tsai et al., 2019). Nevertheless, the main obstacle to limit the application of slope units is the difficulty of automatic and efficient extraction for reasonable slope units using the conventional geographic information system (GIS)-based hydrological analysis method (Xie et al., 2004; Ba et al., 2018). Hence, improving the automation and efficiency of slope unit extraction at a large scale is still a challenging task. Fortunately, an image segmentation method, i.e. multi-scale segmentation (MSS), has achieved the automatic extraction of slope units, as recently introduced by Huang et al. (2021). Although this method has been widely used for landslide detection, classification and other image analysis, the slope units extracted by this method have not been attempted for LSP, and it is needed to fill this gap (Hölbling et al., 2012; Moosavi et al., 2014).

Additionally, another issue relating to the heterogeneity of slope unit-based conditioning factors needs to be successfully resolved in the LSP modeling. Literature suggests that the main slope unit-based conditioning factors include topography, geography, hydrological and land cover factors, which are widely applied for LSP modeling (Reichenbach et al., 2018; Saha et al., 2021). In the past LSP researches using slope units, it can be found that the information of conditioning factors within the slope units are represented and descripted by averaging values. This may cause some errors and oversimplifications in the used multivariate models, because the heterogeneity of conditioning factors within slope units cannot be fully considered (Sun et al., 2019; Tsai et al., 2019). Focusing on this drawback, according to the research results of Catani et al. (2013), the internal variations of conditioning factors can be characterized by resorting to the descriptive statistics variables of mean, range and standard deviation (STD) values of each conditioning factor to obtain more reasonable and abundant slope unit-based conditioning factors.

After that, the slope unit-based conditioning factors combining with the recorded landslides data can be imported into specific machine learning models to construct landslide susceptibility models for LSP. In recent years, the machine learning models have been widely used for LSP and have been proven to have higher prediction accuracy than conventional heuristic models and mathematical statistical models (Reichenbach et al., 2018; Achour and Pourghasemi, 2020). In addition, the machine learning models have a strong nonlinear fitting ability, high tolerance to various types of conditioning factors, certain tolerance to conditioning factor errors and a few parameter settings (Merghadi et al., 2020; Zhang and Phoon, 2022; Zhang et al., 2022a, b, c; Zhu et al., 2022). Among the machine learning models, the multi-layer perceptron (MLP) neural networks can improve the prediction performance due to the strong model flexibility and nonlinear fitting ability, as well as the capability of optimization under complex multi-typological input data (Shirzadi et al., 2017). On the other hand, some literature shows that the random forest (RF) model has higher LSP accuracy, because the RF model has fast training speed to large-scale datasets and can avoid over-fitting by controlling the number of trees (Catani et al., 2013; Youssef et al., 2016; Zhang et al., 2022a, b, c).

Therefore, two machine learning models of MLP and RF are selected to perform LSP in this study. Those two models are combined with slope units to construct Slope-RF and Slope-MLP models, comparing to conventional grid units-based (Grid-RF and Grid-MLP) models. Then the internal variations of conditioning factors are further considered in the Slope unit-based machine learning models to build variant Slope-RF and variant Slope-MLP models. The Chongyi County in China is selected as the case study. A total of fifteen slope unit-based conditioning factors are extracted by averaging the grid unit-based conditioning factors within each slope unit; and then are expanded to 38 slope unit-based conditioning factors through considering the internal variations of conditioning factors. The prediction performances of the above six types of LSP models are assessed through calculating the area under the receiver operating features curve (AUC) and frequency ratio (FR) accuracy. In addition, 19 new landslides (2009–2019) are investigated in the field and recorded to validate the applicability and accuracy of the LSMs once again.

2. Theories of variant slope-based machine learning models

2.1. LSP modeling procedures

The modeling procedures of variant Slope-based machine learning models are shown in Fig. 1. At the first stage, the basic data and landslide inventory are collected and prepared, such as the geological data, Landsat-8 images, field survey data and 235 landslides data. The slope units are extracted using the MSS method, and then the most important original conditioning factors are selected and mapped based on these slope units. At the second stage, two typical machine learning models (RF and MLP) are combined with slope units to construct Slope-RF and Slope-MLP models. Afterwards, the heterogeneity of conditioning factors has been further considered in the Slope-based machine learning models to build variant Slope-RF and variant Slope-MLP models. At the final stage, LSIs are calculated and LSMs are produced using those models. In addition, the AUC value, FR accuracy and new

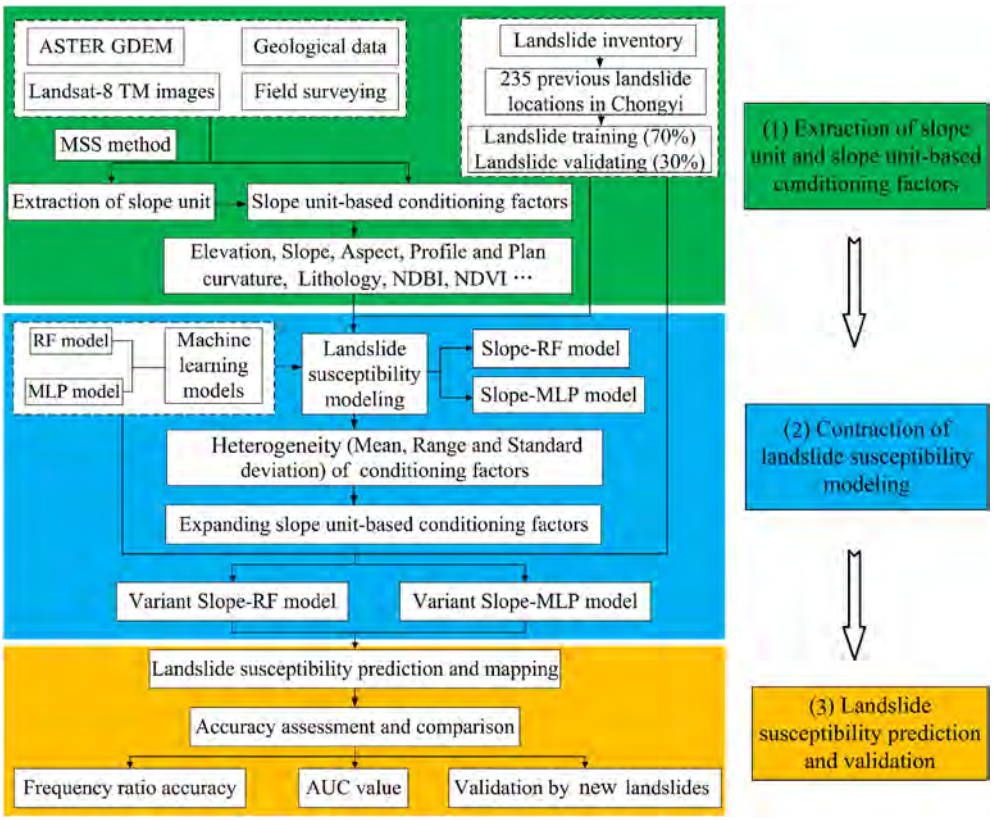

Fig. 1. Flowchart for modeling procedures of variant Slope-based machine learning models.

landslides are applied to assessing the prediction performances of those LSP models.

2.2. Data sources acquisition using 3S technique

The recorded landslides information and landslide-related conditioning factors need to be obtained as the basic data before LSP. At present, the 3S technique including the global position system, remote sensing and GIS has been widely used to obtain the recorded landslides information and conditioning factors (Pradhan, 2010). Generally, remote sensing is mainly used to extract landslide-related conditioning factors. For example, the terrain factors may be extracted from digital elevation models, the land cover factors can be extracted from high-resolution remote sensing images or multi-spectral medium-resolution images. The recorded landslide information about landslide position, areas and boundary are measured through global position systems in field investigation or by aerial and unmanned aerial vehicles photo-interpretation. Afterwards, the landslide inventory is put into GIS software to map landslide surface. A GIS is adopted as the basic platform to capture, store, prepare, analyze and map the data of landslides and conditioning factors for LSP (Zhang et al., 2016).

2.3. Multi-scale segmentation method (MSS)

The MSS method is a novel approach to achieve the automatic and effective extraction of slope units proposed by Huang et al. (2021). This method uses a bottom-up region merging segmentation algorithm to implement the minimum homogeneity between the image objects and the maximum homogeneity within the image objects. The basic principle of the MSS method is to combine pixels with the same features (the shape, color, texture) into an image object to realize the slope unit division. Using the MSS method to extract slope units, selecting the appropriate input images and determining the reasonable segmentation parameter combination play a significant role in the segmentation results. For the former, the segmentation results depend on the input data quality and characteristics such as spatial resolution, image quantization and the scene characteristics (Hölbling et al., 2015). According to the definition of slope unit, the regional aspect and shaded relief maps are selected as the input layers and then combined into a multiband image. For the latter, the parameter combination including scale, shape and compactness parameters can be determined by the improved trial-and-error method, integrating the conventional trial-and-error method with the morphological and scale information of landslides. More details about the slope unit extraction using MSS method are introduced in Huang et al. (2021).

2.4. Heterogeneity of conditioning factors within slope units

The heterogeneity of conditioning factors within a slope unit represents the variability and difference of conditioning factor information at the slope unit scale. In this study, it can be found that some topographic and hydrological conditioning factors (such as elevation, slope, profile curvature and others) show high variability at different locations, while the conditioning factors such as lithology and aspect are usually with little variability in slope units. For the grid unit-based conditioning factors, each grid unit has a certain value for each conditioning factor, and there is some heterogeneity between the grid units at different locations. However, for the slope unit-based conditioning factors, there may be hundreds of grid units with different conditioning factor values within

each slope unit. As a result, a significant heterogeneity exists between those grid units within a certain slope unit.

At present, the values of slope unit-based conditioning factors are generally assigned by the mean and/or majority values of all grid unit values within each slope unit, through the zoning statistical function in the ArcGIS 10.2 software. As a result, the heterogeneity of conditioning factors has not been fully accounted for, resulting in the information loss of conditioning factors. Hence, to enrich the local-scale information and fit the heterogeneity of slope unit-based conditioning factors, the descriptive statistics variables of range values and STD values of slope unit-based conditioning factors are considered as input variables of LSP model. The range variables, defined as the differences between the maximum and minimum values of each grid unit-based conditioning factor within each slope unit, can reflect the variation of the conditioning factor in each slope unit. Meanwhile, the STD variables can reflect the dispersion degree of grid unit-based conditioning factor values in each slope unit. The processes to obtain the range and STD variables are shown in Fig. 2. In this process, for the incomplete grid units in a certain slope unit, if the slope unit contains the central point of incomplete grid units, the conditioning factor data are considered in this slope unit (green point in Fig. 2). Otherwise, it is not considered (red point in Fig. 2).

2.5. Machine learning models

In this study, RF and MLP models are selected as the basic machine learning to construct the Slope- and variant Slope-machine learning models for LSP.

2.5.1. RF

RF model is a powerful ensemble learning technique, which is one of the most prevalent methods to address the problem of classification and prediction by generating many classification trees (Achour and Pourghasemi, 2020). In RF model, the diversities among the decision trees can be well achieved by resampling the data with replacement and randomly changing the predictive variable sets over different tree induction processes (Tsangaratos et al., 2017). In RF model, the Gini index is used to select the variable features. Suppose to classify the samples to T classes, the probability that a sample is in class t is p_t and the corresponding Gini index can be calculated by following equation. The smaller the value of Gini index, the less the uncertainty of data.

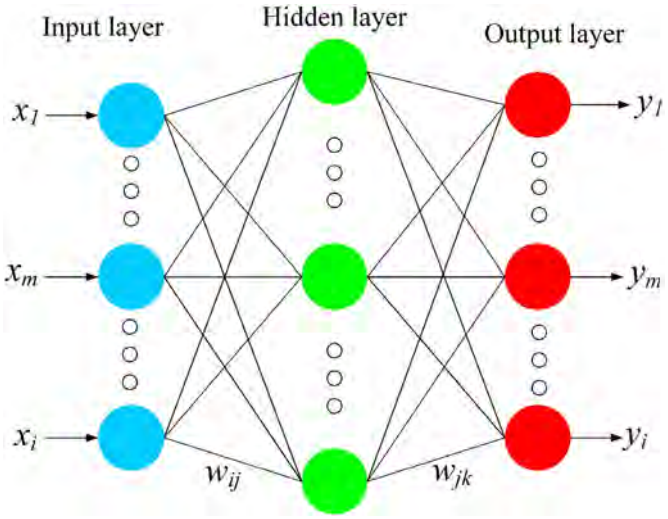

Fig. 3. Flowchart of MLP model.

$$Gini(p) = \sum_{t=1}^{T} p_t(1-p_t) = 1 - \sum_{t=1}^{T} p_t^2$$

To construct the RF model, the conditioning factors of samples are selected as the basic input variables to build the classification tree, the RF model output can represent the probability to one of the possible classes. The performance of RF is mainly determined by two user-defined parameters: k and m. The parameter k can well reflect the information of each decision tree, and the parameter m is used to reflect the total scale of RF. In addition, the generalization error produced during RF model construction can be estimated by out-of-bag (OOB) error, which means that approximately 66% ("in-bag") of the bootstrapped samples are used for the training of each tree, and the remaining 33% ("OOB") are used for evaluating the accuracy of the final ensemble model. The more luxuriant each tree is and the more independent the trees are, the higher the prediction performance RF is. The main processes to construct RF model include three steps: (1) specifying the value of m, which is used to randomly generate m variables for the binary tree on the node through the minimum principle of node impurity; (2) k sample sets from the original data set are randomly extracted with replacement

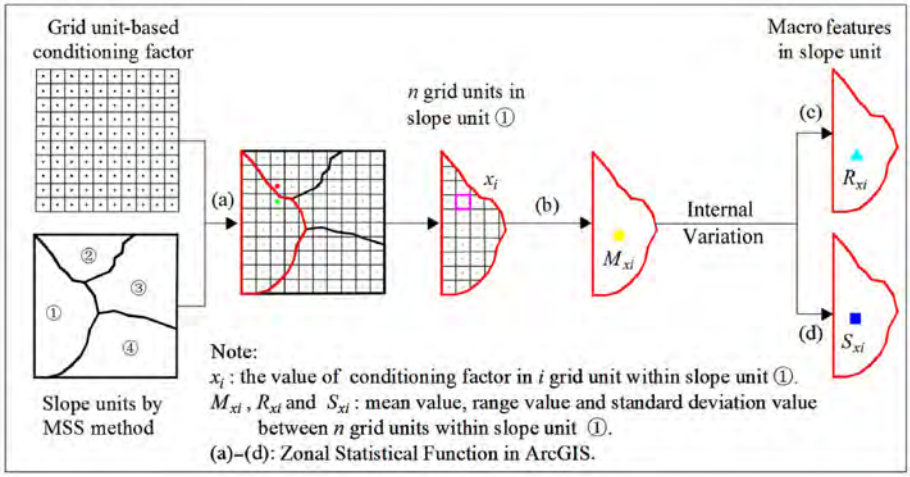

Fig. 2. The process to obtain internal variation variables within slope units.

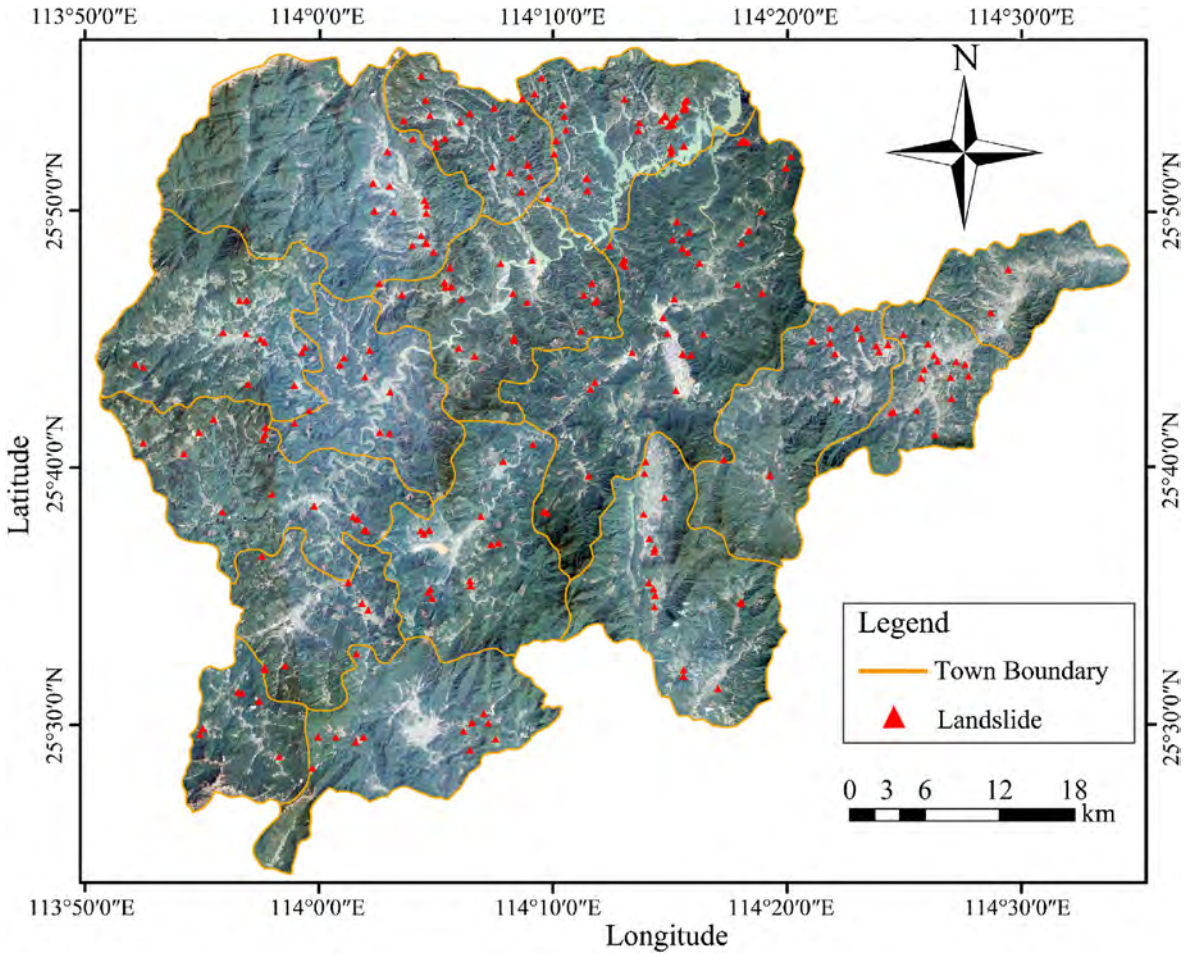

Fig. 4. Satellite image and landslide distribution of Chongyi County.

to form *k* decision trees by utilizing Bootstrap self-help method, while the no extracted samples are used for prediction of a single decision tree; (3) The samples are classified by the principle of voting method or predicted by the principle of simple average using the RF model composed of *k* decision trees.

2.5.2. MLP model

MLP model is a popular neural network that is constructed by three main compositions of input, hidden and output layers. The MLP has a widespread application in the LSP researches in recent years (Bui et al., 2016; Shirzadi et al., 2017). The flowchart of MLP model is shown in Fig. 3. The input layers can be considered as the conditioning factor induced landslides whereas the output layers are viewed as the classified results (landslide and non-landslide). The hidden layers are the classifying layers to transform inputs to outputs, which can be used to cope with the nonlinear classification problems through an activation function (a sigmoid function is generally used) (Pham et al., 2017; Lawal and Kwon, 2021). The input, hidden and output neurons are connected through weights, which are first initialized and then updated using the back-propagation algorithm until the difference between computed and given output is sufficiently small.

The main processes to construct MLP mainly include two steps: (1) the input variables are propagated forward through the hidden layers to produce the output values, and then the differences between output values and pre-values are estimated; and (2) the connection weights are updated through an iterative process based on the back propagation algorithm to optimize the best results with the least difference (Tien Bui et al., 2015). In addition, some advantages exist in the MLP model, for example, the distribution of training dataset is not dependent on pre-assumptions and the most input measurements are selected based on the adjustment of the weight during training process.

2.6. Accuracy assessment of LSP models

It is necessary to verify the prediction performance and to compare the performance of different LSP models (Reichenbach et al., 2018). The receiver operating features curve and FR accuracy validation method are the most common methods to realize these purposes. The receiver operating features curve can be plotted that the horizontal axis is set as 1-specificity and the vertical axis is set as sensitivity (Vakhshoori and Zare, 2018; Darabi et al., 2021). Furthermore, the AUC is generally applied to assessing the prediction performance of LSP models. The larger the AUC value is, the higher the prediction performance is (Cantarino et al., 2018). On the other hand, the FR accuracy is another effective method to evaluate the LSP performance. To calculate the FR accuracy, the LSIs are divided into very low, low, moderate, high and very high landslide susceptibility classes; and then the FR value of each class is calculated. Lastly, the FR accuracy can be calculated by dividing the sum of FR values of high and very high classes by the sum of FR value of very low, low, moderate, high and very high classes (Chang et al., 2020).

3. Study area and landslide inventory

3.1. Study area

The Chongyi County in the southwest part of Jiangxi Province in China is between longitudes of 113°55′–114°38′E and latitudes of 25°24′–25°55′N (Fig. 4). The area covers about 2206.27 km^2, with the length of about 73 km from east to west as well as the width of about 59 km from north to south. The terrain is high in the southeast and low in the northeast. According to the elevation distribution features, the landforms of this study area mainly include valley terrace (≤200 m), hill (200–500 m) and middle-low mountains (≥500 m), respectively accounting for 7.27%, 45.06% and 47.67% of the total area. The elevation ranges from 142 m to 1998 m. The geological units in this region include carbonate rock (limestone), metamorphic rocks (metamorphic fine sandstone and slate), igneous rock (granite) and clasolite rock from Cambrian period to Devonian period. The climatic condition of Chongyi County belongs to sub-tropical monsoon climate with abundant rainfall and humid air. The annual average rainfall in this region is up to 1615.2 mm.

3.2. Landslide inventory information

Based on the results of field investigation and landslide inventory, there are a total of 235 landslides from 1970 to 2003 in the study area (Fig. 4). These landslides can be regarded as shallow landslides with the characteristics of middle and/or small scales and group occurrence. The landslide masses are mainly composed of Quaternary alluvium, and the failure mode is mainly translational and rotational sliding (Hungr et al., 2013). The area of landslides mainly varies between 4.2×10^3 m^2 and 3.2×10^4 m^2 and the average area is about 7.6×10^3 m^2. The thicknesses of landslides vary between 2.8 m and 8 m. The Hengshui Town and Jieba Town located in the northern region have the largest number of landslides, while Longgou Town located in the eastern region has the lowest number of landslides. Furthermore, the shallow landslides are mainly triggered by heavy rainfall.

4. Extraction of slope units and conditioning factors

4.1. Extraction of slope units

In this study, the regional aspect and shaded relief maps (Fig. 5) are extracted from digital elevation model with 8.9 m grid resolution and then taken as the input data in the MSS method. The most appropriate segmentation result is obtained when the scale, shape and compactness parameters are set to 20, 0.8 and 0.8, respectively using the improved trial-and-error method. More details about the determination of those appropriate parameters can be found in Huang et al. (2021). There are 53,055 slope units in Chongyi County. Furthermore, to assess the extraction performance of the MSS method, three cases, i.e. Case 1, Case 2 and Case 3, representing the hill, transition zone and high mountain, respectively, are taken as the study cases (Fig. 5). It can be seen from Fig. 6 that the MSS method has a great extraction performance whatever at high mountain area or hilly area, which can accurately identify the differences between hills to achieve perfectly the extraction of slope units.

4.2. Selection of slope unit-based conditioning factors

The conditioning factors, which can reflect the natural environmental conditions of slopes and affect the slope stability, can be classified into topographic, geological, hydrological, land cover and human activity factors (Reichenbach et al., 2018). There are a total of 15 slope unit-based conditioning factors, including elevation, slope, aspect, plan curvature, profile curvature, relief amplitude, slope unit morphology, lithology, soil thickness, terrain wetness index, distance to river, drainage density, normalized difference vegetation index (NDVI), normalized difference built-up index (NDBI) and road density (Catani et al., 2013; Sur et al., 2020; Tang et al., 2020). These conditioning factors are used to conduct LSP using the Slope-RF and Slope-MLP models. For purpose of assigning values to each slope-based conditioning factor, each grid unit-based conditioning factor map with the resolution of 8.9 m is statistically analyzed using the zonal statistical function tool in the ArcGIS 10.2 software.

In general, the slope unit-based conditioning factors are divided into continuous and discrete categories. For continuous slope unit-based conditioning factors, the mean, range and STD values of each slope unit are calculated using the grid unit-based conditioning factors values within slope units when the internal variations of slope unit-based conditioning factors are considered (Fig. 2). As a result, there are three variables that can be used for LSP for each continuous slope unit-based conditioning factor. The mean value of the grid units in each slope unit is calculated as the conventional slope-based conditioning factors, while the range and STD values of the grid units in each slope unit are calculated as the variant slope unit-based conditioning factors. All those variant slope unit-based conditioning factors are used as the input variables of variant Slope-based RF/MLP models.

It needs to be emphasized that the morphology of slope unit is determined by the geometrical shape of slope unit. As a result, the

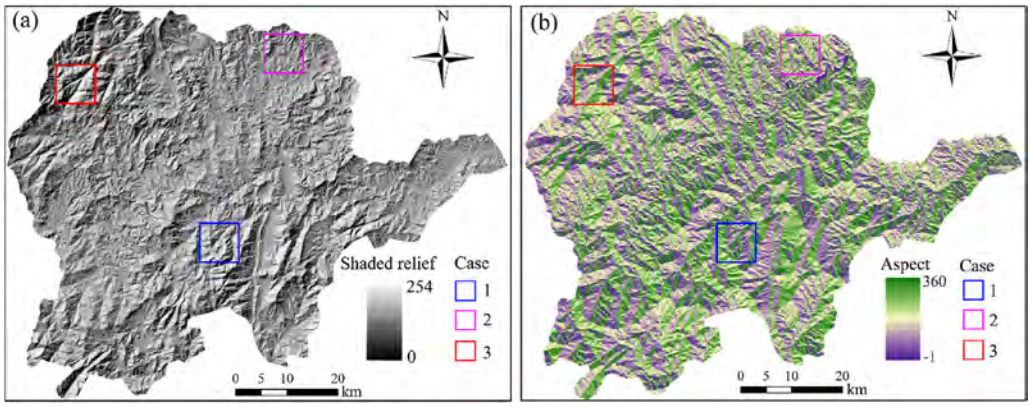

Fig. 5. Shaded relief (a) and aspect (b) (Case 1: hilly zone; Case 2: transition zone; Case 3: high mountain zone).

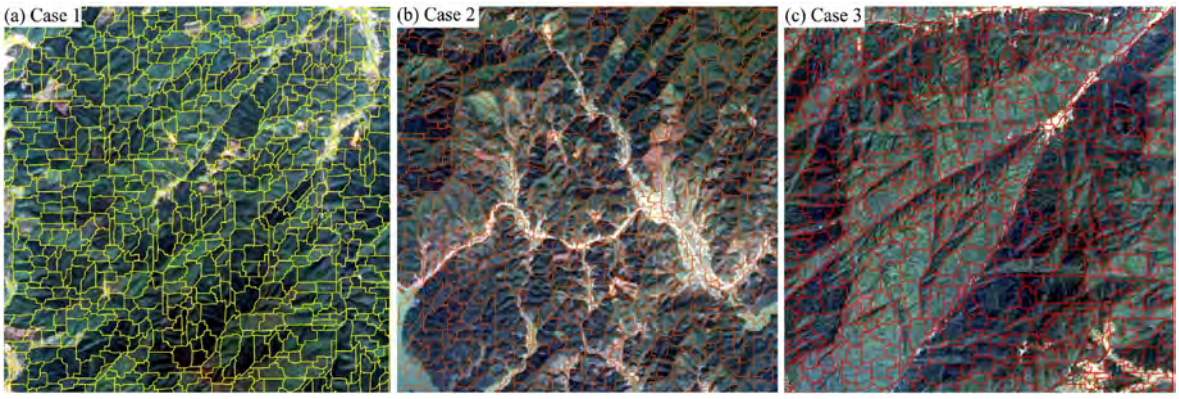

Fig. 6. Slope units of three cases extracted by MSS method.

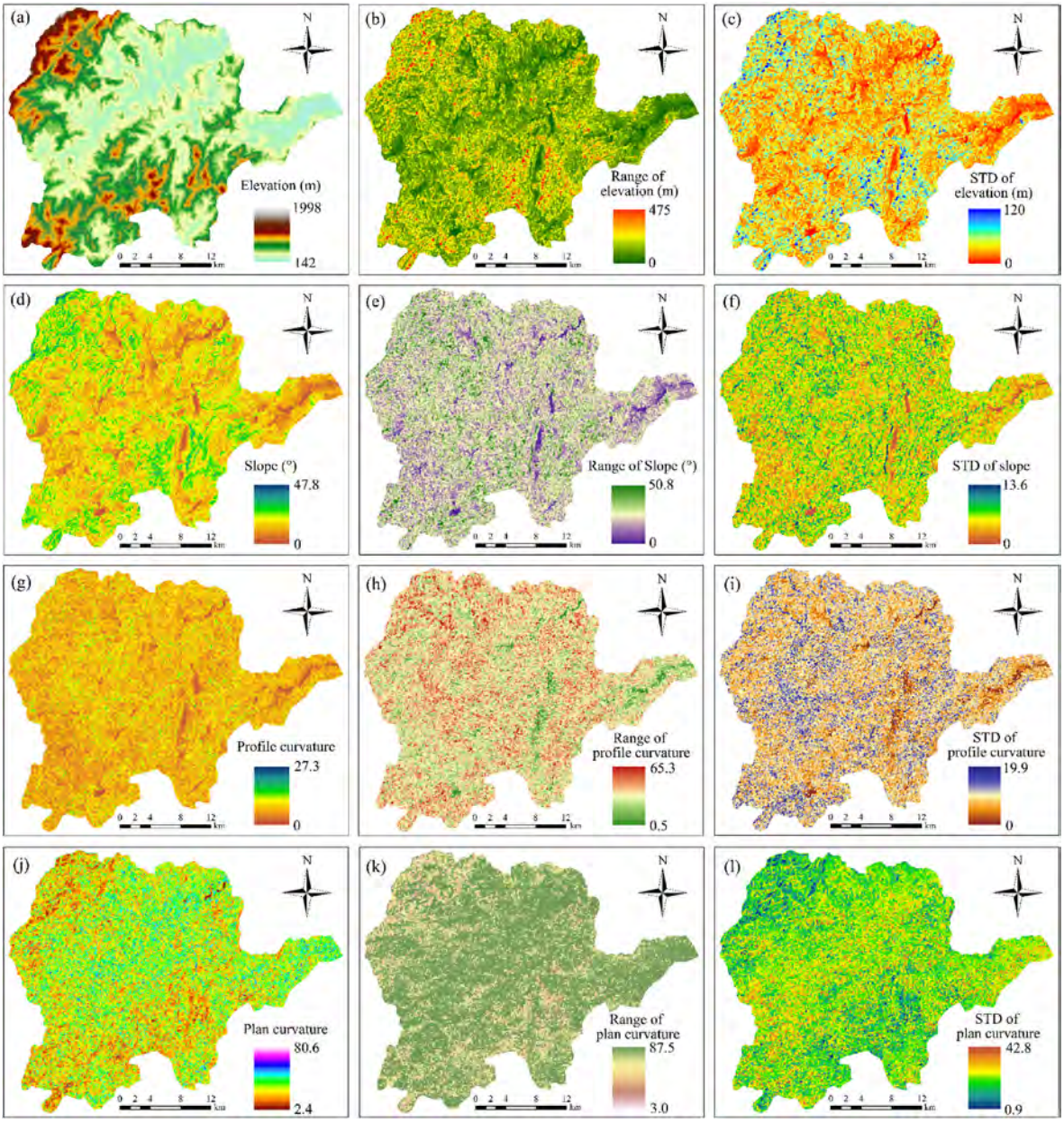

Fig. 7. Topographic conditioning factors: The mean, range and STD of (a, b, c) elevation, (d, e, f) slope, (g, h, i) profile curvature, and (j, k, l) plan curvature.

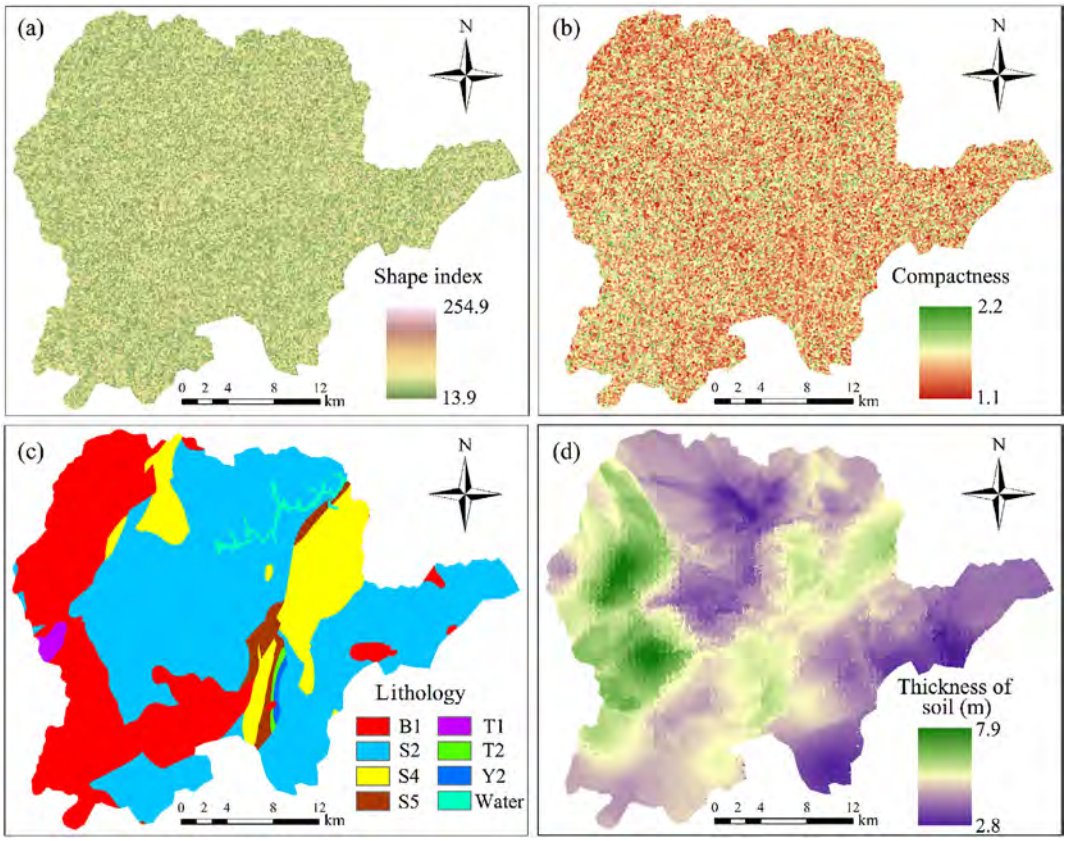

Fig. 8. Conditioning factors of geology and slope unit morphology: (a) Shape index, (b) Compactness, (c) Lithology, and (d) Thickness of soil.

internal variations of the slope morphology have not been considered in this study. In addition, for some discrete slope unit-based conditioning factors, such as lithology, aspect, distance to road and distance to river, it is impossible to adopt range and STD values of each slope unit-based conditioning factor. For example, there may be several lithology types in a slope unit and the mean value of lithology is not existent. Hence, the majority value of each discrete conditioning factor is used as the value of corresponding slope-based conditioning factor. From the above analysis, the original 15 slope unit-based conditioning factors are expanded as a total of 38 expanding slope unit-based conditioning factors for LSP modeling.

4.3. Description of slope unit-based conditioning factors

In this study, the selected slope unit-based conditioning factors of topographic, geological, hydrological, land cover and human activity factors are described as follows.

4.3.1. Topographic factors

The topographic factors of elevation, slope, aspect, plan and profile curvature, slope morphology and relief amplitude are the most basic conditioning factors inducing landslides, which can be extracted through topographic spatial analysis of digital elevation model in the ArcGIS software (Chang et al., 2020; Sur et al., 2020). In order to have a comprehensive and deep understanding about the topographic factors inducing landslides, it is necessary to analyze the variation of topographic factors within slope units. The range and STD values of topographic factors (except aspect and slope morphology) can be calculated, as shown in Fig. 7.

The morphology of slope unit can be quantitatively described by two indicators of shape index value and compactness parameter. Shape index is defined as the ratio of circumference squared to the area. The flatter or more stripe-shaped is, the greater of shape index value is. A shape index value larger than 28 means that the length to width ratio of slope unit is about 5:1. Fig. 8a shows that the shape index ranges from 13.98 to 254.94. The compactness parameter is defined as the ratio of the minimum enclosing rectangle area of a slope unit to the number of pixels it contains. The larger the compactness value is, the more irregular the slope unit is. Fig. 8b shows that the compactness value varies from 1.08 to 2.2.

4.3.2. Geological factors

The lithology is an important conditioning factor for LSP as the basic material of landslide evolution. The lithology map is produced from a geological map with a scale of 1:100,000. The lithology is divided into eight classes: hard clumpy intrusion rock (Y2); limestone and dolomite (T1); slate, metaclastics and phyllite (B1); schist (B2); clumpy chorismite (B3); sandstone, glutenite and mudstone (S2); coal sandstone, shale and mudstone (S4); and sandstone, glutenite and shale (S5) (Fig. 8c). Among above lithology classes, S2 is most widely distributed in the whole area (55.8%), followed by B1 (28.1%) and S4 (11.8%).

The soil thickness, defined as the depth from the surface to the bedrock, is also a non-ignorable factor for LSP, because it determines the slide surface, size and volume of shallow landslides in Chongyi County (Kuriakose et al., 2009; Tufano et al., 2021). The methods to map the soil thickness at the regional scale include physically-based, empirical-statistical, interpolation and machine learning methods (Kuriakose et al., 2009; Catani et al., 2013; Kim and Ji, 2022). Among those methods, the interpolation method

such as Kriging has been widely used in different landscapes for the soil thickness estimation based on the sample point data. Therefore, in this study, the Kriging interpolation method is selected to estimate the soil thickness in the ArcGIS software. The soil thicknesses of 235 landslides have been investigated and recorded as the sample data. Two hundred samples are used to estimate soil thickness and 35 samples are used to validate the estimation performance. Moreover, the mean error and root mean square error are applied to evaluating the estimation performance and efficiency. As a result, the soil thickness of this study area in the slope units ranges from 2.84 m to 7.9 m (as shown in Fig. 8d).

4.3.3. Hydrological factors

It is known that the river streams have a negative influence on slope stability by eroding and absorbing materials at the bottom of slopes (Prashad Bhatt et al., 2013). In this study, the terrain wetness index, drainage density and distance to river are selected as the hydrological factors extracted through the hydrological analysis method in ArcGIS software based on the digital elevation model data. The terrain wetness index is used to reflect the important effects of topography and soil moisture content on landslide occurrence (Fig. 9a). Drainage density can show the balance characteristics between climate, geomorphology and hydrology (Fig. 9b and c). The spatial position relationships between landslides and river streams can be well reflected by the distance to river.

4.3.4. Land cover and human activity factors

The NDVI and NDBI, extracted from Landsat TM 8 images, are two typical conditioning factors that reflect land cover and human activities (Fig. 9d). NDVI is an excellent indicator of local vegetation growth and coverage, which is also related to the landslide occurrence because vegetation can reduce the influence of rainfall on landslides through enhancing the shear strength of the slope soil. At the same time, the NDBI can well reflect the distribution rate of human construction land in the study area (Yang et al., 2019).

Landslides have frequently occurred with an increase of human activities. The main reason is that a large number of roads have been conducted in mountainous areas, and road excavation has changed the topographic environment and stress conditions of slopes along the roads, leading to the decrease of slope stability (Donnini et al., 2017). Hence, the road density has been selected to analyze the impacts of road construction on landslides. The roads in this region are extracted from Google Earth 7.1.8.3036 (32-bit) with a scale of 1:25,000 in vector format. Fig. 9d and e shows that the mean values of the road density vary from 0 to 6.90 km/km^2 and the range values of road density vary between 0 and 5.33 km/km^2.

4.4. Effects of the slope unit-based conditioning factors on landslides

The FR method has been widely used to explore the effects of the conditioning factors on LSP (Lee and Pradhan, 2006). More details of this can be found in Chang et al. (2020). In this study, the slope unit-based conditioning factors are divided into eight classes using the natural break point method (Huang et al., 2020) (the lithology is divided by strata configuration and the aspect is divided into nine classes), and the results of FR method are presented in Table 1. For example, the FR values are greater than 1 when the mean, range and STD values of elevation in the slope units are 142–421 m, 0–78 m and 0–12.27 m, respectively, suggesting that landslides more probably occur in those conditions. About 79.2% of the slope units with landslides are distributed in the lithology of S2, S4 and S5 with the FR values greater than 1.

The correlations between 38 expanding slope unit-based conditioning factors are analyzed to avoid the effect of multicollinearity among those variables. Literature shows that when the absolute value of the correlation coefficient is less than 0.3, the two variables are considered negligible (Mukaka, 2012). The correlation analysis results in the SPSS 22 software show that there are a total of 22 expanding slope unit-based conditioning factors having negligible correlations (the absolute value of the correlation coefficient is less than 0.3), including elevation (mean and range variables), slope (mean, range and STD variables), profile curvature (mean variable), plan curvature (mean, range and STD variables), terrain wetness index (mean variable), NDBI (mean variable), NDVI (mean variable), road density (mean and range variables), drainage

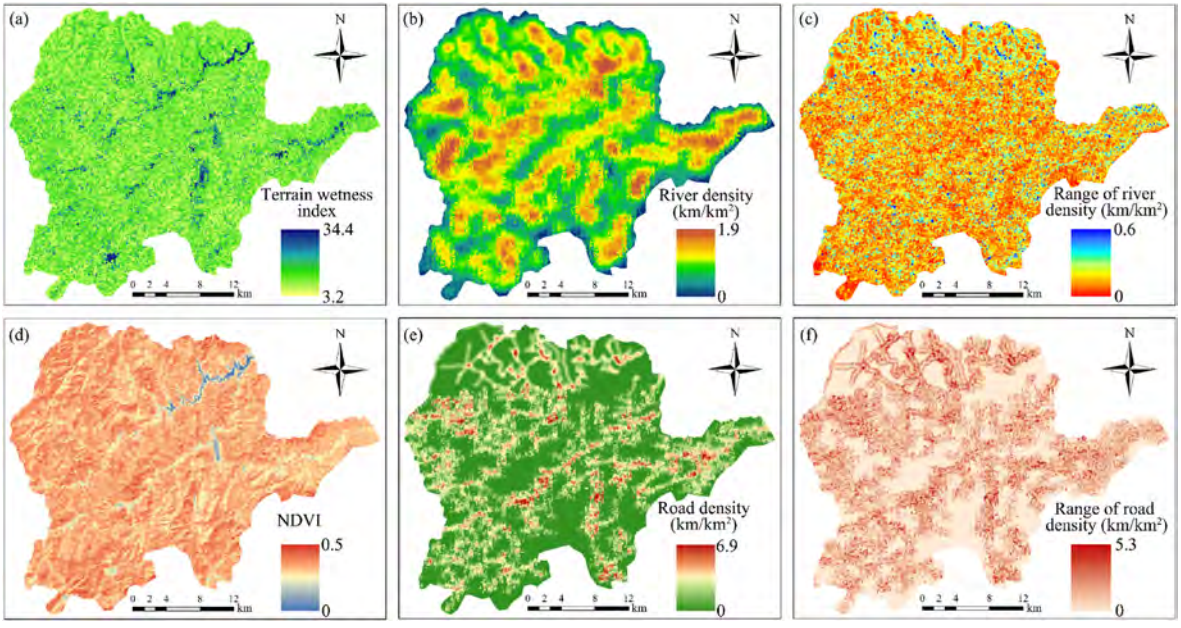

Fig. 9. Conditioning factors of hydrological, land cover and human activity: (a) Terrain wetness index, (b) River density, (c) Range of river density, (d) NDVI, (e) Road density, and (f) Range of road density.

Table 1
FRs of slope unit-based conditioning factors.

Conditioning factor	Resolution/scale	Mean/Majority				Range		STD	
		Class	Ratio of total region	Ratio of landslide	FR	Class	FR	Class	FR
Elevation (m)	8.9 m	142–311	0.175	0.422	2.409	0–31	1.229	0–7.08	1.147
		311–421	0.216	0.233	1.078	31–55	1.168	7.08–12.27	1.282
		421–536	0.191	0.153	0.797	55–78	1.001	12.27–17.47	0.955
		536–669	0.145	0.094	0.646	78–100	0.969	17.47–22.66	0.992
		669–823	0.109	0.058	0.527	100–124	0.716	22.66–27.85	0.933
		823–996	0.089	0.032	0.36	124–151	0.845	27.85–33.05	0.639
		996–1234	0.058	0.009	0.162	151–180	0.724	33.05–39.18	0.76
		1234–1998	0.016	0	0	180–475	0.493	>39.18	0.735
Slope (°)	8.9 m	0–6.38	0.07	0.116	1.674	0–5.38	0.577	0–2.07	0.911
		6.38–10.5	0.16	0.288	1.794	5.38–9.37	1.242	2.07–3.14	1.122
		10.5–13.88	0.193	0.193	0.999	9.37–12.36	1.113	3.14–4.04	0.947
		13.88–17.09	0.193	0.177	0.916	12.36–15.15	0.936	4.04–4.95	1.068
		17.09–20.4	0.159	0.123	0.775	15.15–17.94	1.018	4.95–5.91	0.974
		20.4–24.19	0.119	0.086	0.717	17.94–20.93	0.988	5.91–7.03	0.936
		24.19–29.07	0.074	0.015	0.2	20.93–24.12	1.106	7.03–8.63	0.824
		29.07–47.88	0.027	0.003	0.099	24.12–50.83	0.821	8.63–13.58	0.567
Profile curvature	8.9 m	0.01–3.37	0.048	0.062	1.27	0.55–10.2	0.925	0.07–2.4	1.15
		3.37–5.07	0.144	0.201	1.395	10.2–16.55	1.295	2.40–3.96	1.478
		5.07–6.41	0.186	0.224	1.201	16.55–21.37	1.491	3.96–5.04	1.223
		6.41–7.72	0.195	0.225	1.154	21.37–25.69	1.058	5.04–6.06	1.131
		7.72–9.19	0.175	0.141	0.804	25.69–30.01	0.887	6.06–7.15	1.035
		9.19–11.06	0.137	0.104	0.763	30.01–34.58	1.059	7.15–8.31	0.839
		11.06–13.85	0.084	0.036	0.432	34.58–39.66	0.853	8.31–9.71	0.8
		13.85–27.31	0.031	0.008	0.257	39.66–65.31	0.782	9.71–19.9	0.466
Plan curvature	8.9 m	2.44–14.91	0.064	0.05	0.775	3.02–50.71	0.237	0.88–12.72	0.729
		14.91–20.43	0.118	0.106	0.899	50.71–58.32	0.771	12.72–16.83	0.759
		20.43–25.41	0.146	0.178	1.221	58.32–64.61	0.758	16.83–20.28	1.18
		25.41–30.41	0.165	0.175	1.064	64.61–70.24	0.677	20.28–23.08	1.19
		30.41–35.79	0.167	0.187	1.123	70.24–75.54	0.878	23.08–25.88	1.152
		35.79–42.12	0.15	0.155	1.033	75.54–80.51	0.749	25.88–29.17	0.812
		42.12–50.66	0.121	0.108	0.895	80.51–84.81	1.116	29.17–33.61	0.709
		50.66–80.59	0.07	0.04	0.578	84.81–87.46	1.112	33.61–42.82	0.282
NDBI	1:25,000	0.1–0.28	0.073	0.015	0.203	0–0.13	0.208	0–0.03	0.218
		0.28–0.35	0.172	0.071	0.413	0.13–0.21	0.387	0.03–0.05	0.377
		0.35–0.4	0.203	0.124	0.614	0.21–0.28	0.595	0.05–0.06	0.643
		0.4–0.46	0.202	0.181	0.894	0.28–0.36	1.079	0.06–0.08	1.22
		0.46–0.52	0.178	0.254	1.429	0.36–0.45	1.783	0.08–0.11	1.653
		0.52–0.61	0.102	0.201	1.975	0.45–0.55	2.411	0.11–0.13	2.385
		0.61–0.75	0.049	0.112	2.306	0.55–0.66	2.974	0.13–0.16	2.432
		0.75–1	0.022	0.041	1.875	0.66–0.93	2.955	0.16–0.34	2.601
NDVI	1:25,000	0.01–0.14	0.01	0.005	0.512	0–0.06	0.292	0–0.01	0.197
		0.14–0.23	0.025	0.033	1.337	0.06–0.09	0.424	0.01–0.02	0.563
		0.23–0.28	0.082	0.157	1.911	0.09–0.12	0.763	0.02–0.03	0.856
		0.28–0.31	0.176	0.273	1.554	0.12–0.15	1.156	0.03–0.038	1.166
		0.31–0.33	0.224	0.248	1.104	0.15–0.18	1.505	0.038–0.045	1.545
		0.33–0.36	0.217	0.178	0.82	0.18–0.22	2.128	0.045–0.055	1.851
		0.36–0.39	0.18	0.094	0.519	0.22–0.27	2.271	0.055–0.067	2.019
		0.39–0.48	0.085	0.012	0.142	0.27–0.34	1.26	0.067–0.160	1.146
Relief amplitude (m)	8.9 m	1.21–31.21	0.053	0.089	1.676	0.84–23.52	1.194	0.19–5.4	1.147
		31.21–51.22	0.149	0.307	2.07	23.52–34.86	1.117	5.4–8.38	1.106
		51.22–67.47	0.195	0.214	1.101	34.86–46.21	0.961	8.38–11.11	0.914
		67.47–83.72	0.203	0.172	0.845	46.21–57.55	0.88	11.11–14.34	0.889
		83.72–99.97	0.162	0.115	0.712	57.55–70.78	0.942	14.34–17.82	1.032
		99.97–119.9	0.125	0.074	0.589	70.7–84.9	1.097	17.82–21.79	1.158
		119.9–142.4	0.07	0.026	0.368	84.9–101.9	1	21.79–26.51	0.854
		142.4–320	0.043	0.003	0.060	101.9–241.8	0.338	26.51–63.51	0.338
River density (km/km^2)	8.9 m	0–0.43	0.057	0.009	0.157	0–0.04	0.681	0–0.01	0.718
		0.43–0.63	0.12	0.041	0.346	0.04–0.08	0.934	0.01–0.019	0.922
		0.63–0.8	0.168	0.128	0.76	0.08–0.11	1.082	0.019–0.02	1.074
		0.8–0.96	0.186	0.22	1.183	0.11–0.14	1.088	0.02–0.03	1.197
		0.96–1.11	0.164	0.171	1.041	0.14–0.18	1.393	0.03–0.04	1.31
		1.11–1.28	0.149	0.182	1.22	0.18–0.22	1.181	0.04–0.05	1.048
		1.28–1.47	0.109	0.171	1.561	0.22–0.27	1.171	0.05–0.07	1.463
		1.47–1.95	0.047	0.079	1.687	0.27–0.6	0.959	0.07–0.16	0.9
Road density (km/km^2)	1:25,000	0–1.37	0.676	0.292	0.432	0–0.77	0.617	0.05–0.11	0.512
		1.37–1.83	0.104	0.141	1.36	0.77–1.02	1.369	0.11–0.18	1.243
		1.83–2.29	0.075	0.146	1.941	1.02–1.29	1.597	0.18–0.26	1.358
		2.29–2.78	0.058	0.154	2.646	1.29–1.56	1.893	0.26–0.33	1.711
		2.78–3.32	0.041	0.128	3.158	1.56–1.86	1.896	0.33–0.41	1.568
		3.32–3.94	0.027	0.083	3.026	1.86–2.19	2.204	0.41–0.5	1.838
		3.94–4.75	0.015	0.047	3.1	2.19–2.63	3.713	0.5–0.62	2.344
		4.75–6.89	0.005	0.01	2.176	2.63–5.33	4.284	0.62–1.28	4.02
Terrain wetness index	8.9 m	3.21–4.8	0.127	0.043	0.336	0–4.2	0.36	0–0.76	0.463

Table 1 (*continued*)

Conditioning factor	Resolution/scale	Mean/Majority				Range		STD	
		Class	Ratio of total region	Ratio of landslide	FR	Class	FR	Class	FR
		4.80–5.29	0.213	0.112	0.527	4.2–5.88	0.494	0.76–1.08	0.473
		5.29–5.78	0.242	0.248	1.027	5.88–7.56	0.768	1.08–1.35	0.699
		5.78–6.26	0.164	0.193	1.171	7.56–9.25	1.08	1.35–1.68	1.104
		6.26–7	0.13	0.202	1.549	9.25–11.26	1.175	1.68–2.06	1.443
		7–7.85	0.067	0.099	1.481	11.26–13.28	1.811	2.06–2.49	1.635
		7.85–8.83	0.031	0.068	2.213	13.28–15.64	1.96	2.49–2.98	1.774
		8.83–34.38	0.026	0.035	1.362	15.64–42.87	1.532	2.98–3.68	1.361
Soil thickness (m)	8.9 m	2.84–3.75	0.077	0.084	1.087	0–0.05	0.707	0–0.01	0.746
		3.75–4.25	0.171	0.187	1.097	0.05–0.13	1.482	0.01–0.04	1.594
		4.25–4.68	0.214	0.227	1.064	0.13–0.23	1.413	0.04–0.07	1.18
		4.68–5.1	0.198	0.169	0.855	0.23–0.36	1.487	0.07–0.11	1.423
		5.1–5.52	0.15	0.138	0.924	0.36–0.52	0.887	0.11–0.17	1.206
		5.52–5.97	0.097	0.114	1.176	0.52–0.73	0.886	0.17–0.24	0.476
		5.97–6.63	0.069	0.043	0.621	0.73–1.04	0.609	0.24–0.34	0.926
		6.63–7.9	0.025	0.037	1.472	1.04–1.41	0	0.34–0.55	0
Distance to river (m)	8.9 m	100	0.054	0.076	1.411				
		200	0.243	0.434	1.786				
		300	0.147	0.209	1.421				
		400	0.139	0.115	0.827				
		500	0.119	0.075	0.628				
		600	0.094	0.046	0.484				
		700	0.041	0.013	0.326				
		>700	0.162	0.032	0.198				
Aspect	8.9 m	Plain	0.001	0	0				
		N	0.052	0.023	0.437				
		NE	0.154	0.139	0.906				
		E	0.159	0.183	1.155				
		SE	0.142	0.118	0.829				
		S	0.111	0.102	0.917				
		SW	0.119	0.155	1.301				
		W	0.125	0.146	1.171				
		NW	0.138	0.134	0.973				
Lithology	1:100,000	B1	0.281	0.199	0.707				
		S2	0.558	0.637	1.142				
		S4	0.118	0.128	1.083				
		S5	0.021	0.027	1.274				
		T1	0.007	0.006	0.985				
		T2	0.002	0.001	0.607				
		Y2	0.003	0.001	0.493				
		Water	0.01	0	0				
R value		13.98–17.76	0.07	0.067	0.953				
		17.76–20.59	0.249	0.295	1.182				
		20.59–23.43	0.286	0.309	1.079				
		23.43–26.26	0.178	0.151	0.85				
		26.26–30.04	0.116	0.114	0.981				
		30.04–34.76	0.056	0.037	0.666				
		34.76–40.43	0.025	0.018	0.726				
		40.43–46.1	0.019	0.009	0.475				
Compactness		1.08–1.25	0.107	0.094	0.881				
		1.25–1.36	0.153	0.185	1.211				
		1.36–1.46	0.174	0.185	1.059				
		1.46–1.56	0.171	0.181	1.057				
		1.56–1.67	0.148	0.146	0.986				
		1.67–1.79	0.117	0.096	0.816				
		1.79–1.95	0.083	0.076	0.915				
		1.95–2.19	0.046	0.037	0.812				

density (mean and range variables), soil thickness (mean variable), shape index (mean variable), compactness (mean variable), aspect, lithology and distance to river. Hence, those 22 expanding slope unit-based conditioning factors are used as input variables to implement the LSP using variant Slope-RF and Slope-MLP models.

4.5. Preparation training and validation dataset

It is indispensable to prepare a dataset including conditioning factors and labeled data for machine learning model construction. Then this dataset is divided into training and testing datasets with a certain ratio. The training dataset is generally applied to building LSP models, and the testing dataset is used to validate the prediction performance of LSP models (Merghadi et al., 2020). The labeled data consists of landslide data with a labeled value of 1 and non-landslide data with a labeled value of 0. In this study, there are a total of 744 landslide slope units where landslides have occurred that are labeled to 1, and a same number of non-landslide slope units, which are randomly sampled from the landslide-free area, are labeled to 0. Afterwards, the dataset including slope unit-based conditioning factors and labeled data is randomly spilt into a training dataset and a testing dataset with a ratio of 70%/30%. The training dataset is used to construct the LSP models and the testing dataset is used to verify the predictive accuracies of LSP models.

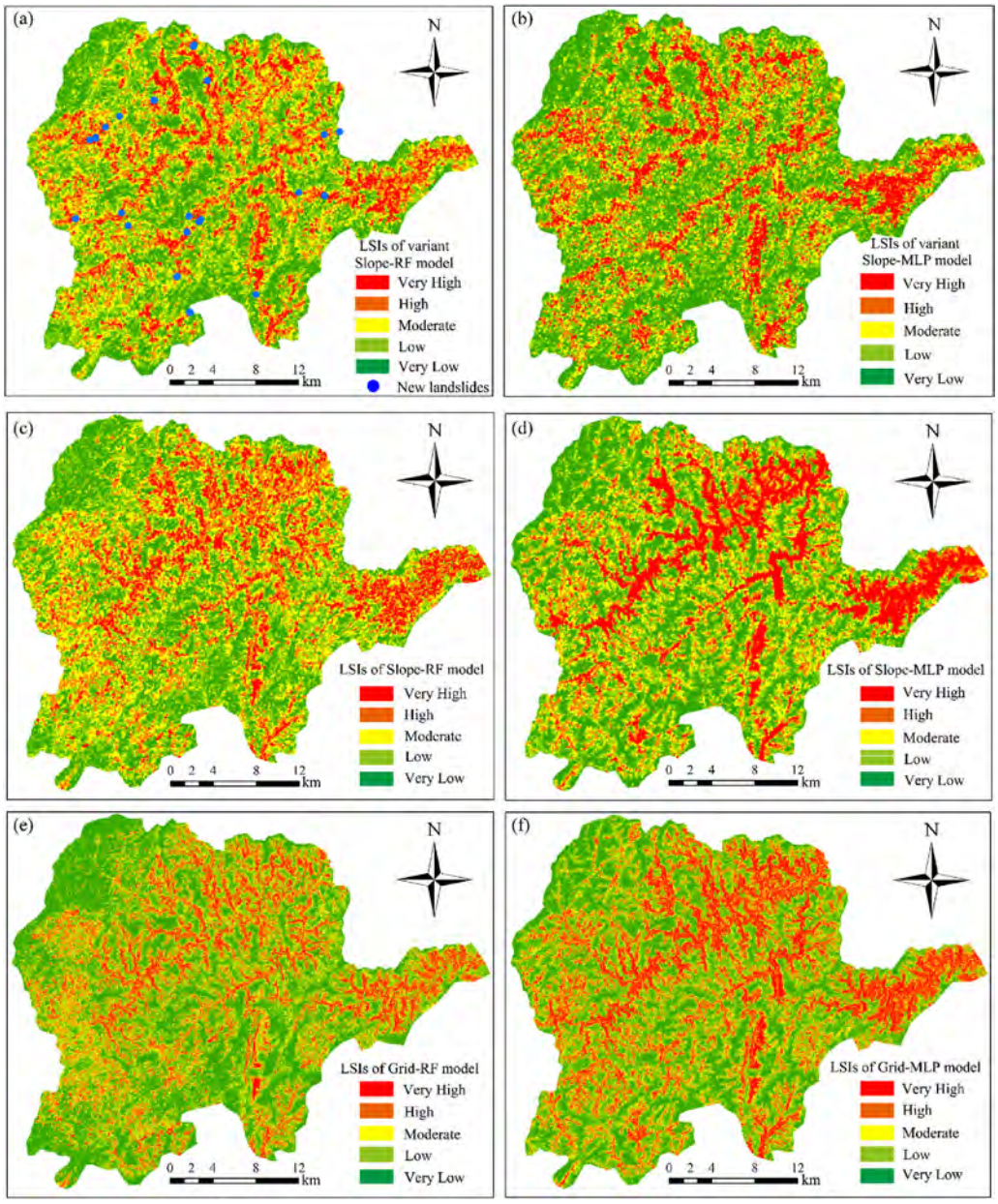

Fig. 10. LSMs of different RF and MLP models.

4.6. Construction of LSP modeling

In the processes of LSP modeling, 15 slope unit-based conditioning factors are selected as input variables to construct conventional Slope-machine learning models, and 22 expanding slope unit-based conditioning factors are used as input variables to construct variant Slope-machine learning models. The FR values for each conditioning factor of training samples (landslide and non-landslide samples) are used as the basic input data to construct RF and MLP models. As for RF models, the statistical package R version 3.8 is applied for building of variant Slope-RF and Slope-RF models. The number of trees in RF has been fixed to 500 after a primary analysis, and the number of samples at each node has been set as 3 to analyze the joint contribution of subsets of features and to keep a fast convergence during iterations. As for MLP models (variant Slope-MLP and Slope-MLP), three-layer models with one input layer, one hidden layer and one output layer are also used for LSP. The sigmoid function is selected as the activation function and the back-propagation algorithm is used to train the MLP models.

5. Results

5.1. LSMs of the RF and MLP models

In this study, the LSMs of RF and MLP models are mapped, and then the LSIs are divided into five classes using the natural break point method in ArcGIS 10.2 software, which is a classified method according to the numerical statistical distribution by maximizing the difference between different classes (Merghadi et al., 2020; Pham et al., 2019). The LSMs of the variant Slope-RF and Slope-MLP models are shown in Fig. 10a and b, respectively. It can be seen from Fig. 10a that the very low, low, moderate, high and very high susceptibility classes cover 25.94%, 26.67%, 21.79%, 16.48% and 9.13% of the variant Slope-RF model, respectively. Meanwhile, Fig. 10b

shows that the very low, low, moderate, high and very high susceptibility classes cover 37.45%, 23.04%, 15.77%, 12.40% and 11.34% of the variant Slope-MLP model, respectively. In addition, the LSMs of the Slope-RF, Slope-MLP, Grid-RF and Grid-MLP models are shown in Fig. 10c–f, respectively. Furthermore, compared with the LSMs of the Grid-RF and Grid-MLP models, it can be found that the LSMs based on slope units have stronger practical application than that based on grid units. For example, the location and scope where landslide with very high susceptibility class is prone to occur by the Slope-machine learning models can be accurately recognized and easily found in practice. In addition, the error that caused by isolated grid units with very high landslide susceptibility class in Grid-machine learning models also can be avoided using the Slope-machine learning models.

5.2. Validation of LSP

The AUC value of receiver operating feature curve and FR accuracy validation method are introduced for evaluating the LSP performance of LSP models.

5.2.1. The AUC value of receiver operating features curve

The receiver operating feature curves of the LSP models are shown in Fig. 11. The AUC values of the variant Slope-RF, Slope-RF, Grid-RF, variant Slope-MLP, Slope-MLP and Grid-MLP models are 0.875, 0.827, 0.896, 0.843, 0.805 and 0.826, respectively. It can be concluded that the prediction performances of the variant Slope-RF and variant Slope-MLP models are better than those of the Slope-RF and Slope-MLP models. The Grid-RF model has a better prediction performance than the Grid-MLP model. Meanwhile, it is revealed that the RF models have better prediction performance than that of the MLP models.

5.2.2. FR accuracy validation

In this study, the FR accuracies of the RF and MLP models are shown in Table 2. The FR values in the MLP models decrease from very high to very low susceptibility classes. However, the FR values in the RF models exhibit the characteristic that the FR values of the very high susceptibility class are significantly larger than that of other four susceptibility classes. Furthermore, the FR accuracies of the variant Slope-RF, Slope-RF, Grid-RF, variant Slope-MLP, Slope-MLP and Grid-MLP are 0.958, 0.948, 0.974, 0.762, 0.751 and 0.77, respectively. Therefore, it appears that the LSP accuracies of variant Slope-machine learning models are better than that of Slope-machine learning models, suggesting that the LSP predictions in consideration of the internal variation of the conditioning factors within slope units are more in line with the observations. It can also be found that the LSP accuracy based on the slope unit is close to that based on the grid unit. Furthermore, the comparisons also show that the prediction performances of the RF models are superior to those of MLP models according to the used criteria.

Table 2
FR among the landslide susceptibility classes for different LSP models.

LSP model	Class	Threshold of each class	Percentage of slope unit/grid in domain	Percentage of landslide slope unit/grid	FR
Variant Slope-RF	Very high	[0.69, 0.99]	0.091	0.793	8.692
	High	[0.52, 0.69)	0.165	0.111	0.674
	Moderate	[0.37, 0.52)	0.218	0.059	0.273
	Low	[0.23, 0.37)	0.267	0.028	0.107
	Very low	[0.02, 0.23)	0.259	0.008	0.03
Slope-RF	Very high	[0.73, 0.99]	0.096	0.714	7.407
	High	[0.54, 0.73)	0.176	0.175	0.994
	Moderate	[0.36, 0.54)	0.233	0.067	0.288
	Low	[0.19, 0.36)	0.268	0.033	0.125
	Very low	[0.01, 0.19)	0.226	0.011	0.047
Grid-RF	Very high	[0.69, 1]	0.091	0.854	9.696
	High	[0.49, 0.69)	0.141	0.091	0.646
	Moderate	[0.31, 0.49)	0.186	0.032	0.138
	Low	[0.15, 0.31)	0.243	0.015	0.037
	Very low	[0, 0.15)	0.338	0.007	0.006
Variant Slope-MLP	Very high	[0.74, 0.96]	0.113	0.417	3.68
	High	[0.55, 0.74)	0.124	0.235	1.896
	Moderate	[0.36, 0.55)	0.158	0.168	1.065
	Low	[0.19, 0.36)	0.23	0.116	0.505
	Very low	[0.03, 0.19)	0.374	0.063	0.169
Slope-MLP	Very high	[0.68, 0.85]	0.133	0.439	3.3
	High	[0.53, 0.68)	0.139	0.222	1.604
	Moderate	[0.4, 0.53)	0.166	0.154	0.926
	Low	[0.28, 0.4)	0.257	0.141	0.548
	Very low	[0.13, 0.28)	0.306	0.044	0.145
Grid-MLP	Very high	[0.67, 0.92]	0.152	0.487	3.209
	High	[0.51, 0.67)	0.174	0.239	1.37
	Moderate	[0.35, 0.51)	0.174	0.143	0.821
	Low	[0.2, 0.35)	0.236	0.099	0.42
	Very low	[0.03, 0.2)	0.265	0.033	0.124

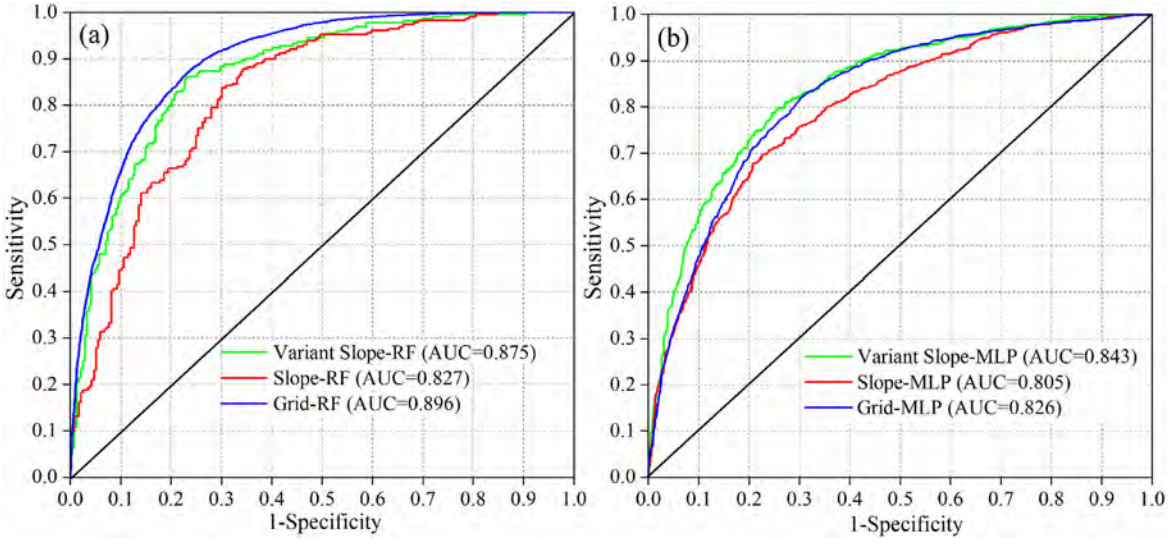

Fig. 11. The receiver operating feature curves and AUC values of (a) RF and (b) MLP models.

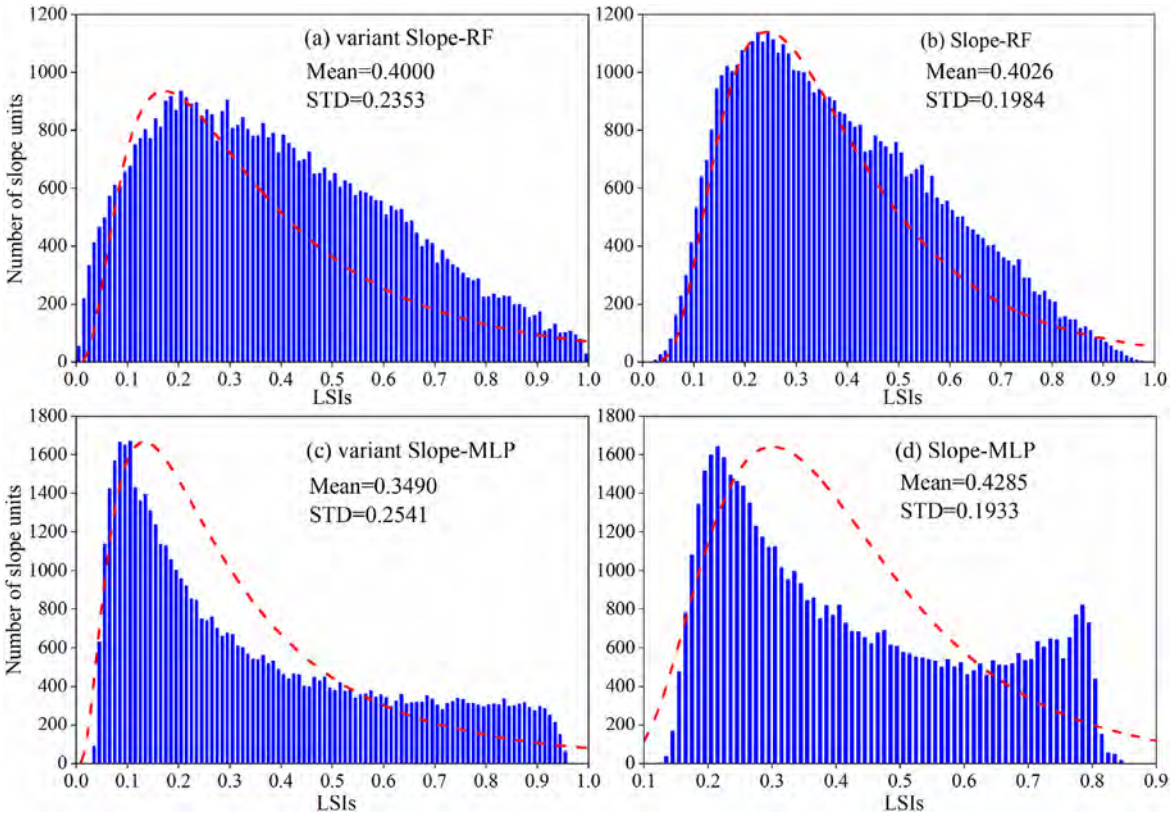

Fig. 12. LSI distribution features of (variant) Slope-RF and Slope-MLP models.

6. Discussion

6.1. Comparison of the LSP performance for the RF and MLP models

The validation results through the AUC values and FR accuracy indicate that the RF models have a much better LSP performance than the MLP models. This is attributed to the essential differences of the classification algorithm between the RF and MLP models. The RF algorithm is a supervised classification algorithm and is an ensemble method using decision tree models that each tree fits a data subset sampled independently using bootstrapping. There are some advantages resulting in excellent performance in the field of pattern recognition:

(1) It is simple and has high accuracy due to the ensemble algorithm.
(2) Over-fitting can be avoided by building large forests, portraying observations with replacements (i.e. bootstrapped) and splitting the nodes on the best split within a random subset (Merghadi et al., 2020).
(3) RF can provide high accuracy rates with respect to the outliers of the predictors due to the use of random selection at each split node depending on the two data objects of OOB and proximities (Breiman, 2001).
(4) It has strong adaptability to datasets. For example, a dataset with high dimensions can be processed without feature selection, and both discrete and continuous data can be processed without normalization.
(5) Some hyper-parameters, including the number of trees, the maximum depth of the trees and the maximum number of features considered at each split, can be tuned to implement the best classification performance.

In the MLP models, the selection of the number of implicit nodes and the determination of some parameters (stopping threshold, learning rate and activation function) have become the main problems that restrict the application of MLP models.

6.2. Frequency distribution of LSI values

The distribution features of the LSIs are analyzed and compared to understand the LSP results more comprehensively. The LSI distributions of the variant Slope-RF, Slope-RF, variant Slope-MLP and Slope-MLP models with their corresponding mean and STD values are shown in Fig. 12. The mean values reflect the centralization trend of the LSIs, and the STD values reflect the dispersion degree of the LSIs. It can be seen from Fig. 12 that the distribution patterns of the LSIs for Slope-based RF and MLP models conform to approximate logarithmic normal distributions (red line in Fig. 12). The LSIs calculated by the RF and MLP models mainly belong to low and very low landslide susceptibility classes with a low degree of dispersion. In addition, the mean and STD values suggest that the variant Slope-RF and variant Slope-MLP models have better LSP performance than the Slope-RF and Slope-MLP models. For example, in the results of the RF models, the mean values of the variant slope-RF model and Slope-RF model are close; however, the STD value of the variant Slope-RF model is larger than that of the Slope-RF model.

6.3. Validation analysis by new landslides

After obtaining the LSMs, it is necessary and indispensable to verify the applicability and accuracy of the results in practice. In this study, some new landslides have been recorded and used to verify the prediction performance of variant Slope-RF, Slope-RF, variant

Slope-MLP and Slope-MLP models. First, 19 new landslides in the period from 2009 to 2019 have been investigated in the field and recorded in Table 3 and Fig. 10a. Then, the LSMs produced by variant Slope-RF, Slope-RF, variant Slope-MLP and Slope-MLP models are selected for comparison with those new landslides. Furthermore, the serial number of slope units that generated new landslides and the corresponding slope unit's landslide susceptibility class are recorded in Table 3.

It can be seen form Table 3 that among those slope units with new landslides, the number of slope units with very high landslide susceptibility class of variant Slope-RF, Slope-RF, variant Slope-MLP and Slope-MLP models are 13, 5, 12 and 8, respectively. The number of slope units with high landslide susceptibility class of variant Slope-RF, Slope-RF, variant Slope-MLP and Slope-MLP models are 4, 10, 5 and 7, respectively. However, there are also two slope units with moderate landslide susceptibility class whatever in variant Slope-RF or variant Slope-MLP models, and four slope units with moderate landslide susceptibility class whatever in Slope-RF or Slope-MLP models. The proportion of new landslides with very high and high landslide susceptibility levels to all new landslides is defined as the predictive accuracy. Hence, the predictive accuracies of variant Slope-RF, Slope-RF, variant Slope-MLP and Slope-MLP models are 0.895, 0.798, 0.895 and 0.798, respectively. The results indicate that more new landslides occurred in the slope units with very high landslide susceptibility class in variant Slope-RF/MLP models than that of Slope-RF/MLP models. Hence, it can be concluded that the LSP results of the variant Slope-RF model have higher applicability and accuracy, and can be used to support the decision-making process for the landslide prevention and mitigation.

6.4. Comparison of LSP results for variant slope, slope and grid-machine learning models

The application of slope unit for LSP is restricted not only by the difficulty of efficient slope unit extraction, but also by the lack of deep understanding about the differences of the LSP results between slope units and grid units. In this study, it has been proved that the MSS method can efficiently and automatically extract slope units in a large scale with high accuracy, which can strongly promote the application of slope units in LSP. On the other hand, Fig. 11 shows that the AUC value of Grid-RF model is slightly higher than that of Slope-RF models, and the similar results also have been revealed in Wang et al. (2017) and Tsai et al. (2019). This is because that more labeled landslide samples are used to construct LSP models when using the grid units than that using the slope units. Moreover, the uncertainties of the non-landslide samples selection and the different machine learning models may also have different effects on the LSP results for Grid- and Slope-based models. Comparing the LSP results of Grid- and Slope-based machine learning models, it can be found that some areas with low and very low susceptibility levels in Grid-based machine learning models may have generally almost isolated grid units with very high and high susceptibility levels; however, this phenomenon can be avoided in the Slope-based machine learning models. Hence, it is incomplete and inconclusive to compare the LSP results only using the AUC value.

Through the comprehensive comparison analysis of the LSP results, it can be revealed that the slope unit is more suitable for the mapping unit of LSP comparing to the grid unit. The main reason is that the LSMs by Slope-machine learning models can be used to accurately determine the definite location and boundary with very high susceptibility class on a slope or basin scale, while the LSMs by the Grid-machine learning models show the features of dispersion and poor discrimination. Another reason is that the computational burden of the Slope-machine learning models is reduced through converting millions of grid units to tens of thousands of slope units (Camilo et al., 2017). Furthermore, slope units can efficiently express the physical relationships between landslides and regional morphological elements, and can guarantee the accurate expression of the information integrity of conditioning factors when compared with grid units (Wang et al., 2005).

Additionally, the variant Slope-machine learning models have more advantages for LSP comparing to the Slope-machine learning models. In fact, a slope unit may contain dozens or hundreds of grid units; as a result, it is biased and incomplete when using only the mean value of each grid unit-based conditioning factor as the value of the slope unit-based conditioning factor. Meanwhile, the heterogeneous features of the slope unit-based conditioning factor cannot be comprehensively considered by the mean value of grid units. Moreover, in the variant Slope-machine learning models, the ranges and STD values can effectively reflect the heterogeneity of

Table 3
New landslides in the period of 2009–2019.

Landslide	Serial number of slope unit	Time of occurrence	LSP class			
			Variant Slope-RF	Slope-RF	Variant Slope-MLP	Slope-MLP
Dapotou landslide	53054	2014/4/28	Very high	Very high	Very high	Very high
Dahedong landslide	6124	2013/5/16	Very high	Very high	Very high	Very high
Modaokeng landslide	16319	2013/8/26	Very high	High	Very high	High
Jinkeng landslide	1330	2015/11/17	High	Moderate	High	Moderate
Changlongkeng landslide	31079	2018/6/9	Very high	Very high	Very high	Very high
Hailuo landslide	12531	2016/6/18	Moderate	Moderate	Moderate	Moderate
Keshulin #1 landslide	35667	2014/8/11	Very high	High	High	High
Shishi landslide	36548	2014/7/14	Very high	High	Very high	High
Keshulin #2 landslide	35651	2019/7/25	High	High	Very high	Very high
Nanliu landslide	13534	2017/7/19	High	High	High	High
Baishikeng landslide	34379	2018/6/17	Very high	Very high	Very high	Very high
Shipotou landslide	37775	2019/5/21	Very high	High	Very high	High
Shuxia landslide	16637	2017/6/18	Very high	High	Very high	Very high
Shangbu landslide	15548	2016/8/27	High	Moderate	High	Moderate
Donglin landslide	29698	2019/5/21	Moderate	Moderate	Moderate	Moderate
Wanglingwan landslide	33003	2018/6/16	Very high	High	Very high	High
S230 K247 landslide	46800	2016/8/28	Very high	High	High	High
Zhangshuxia landslide	34024	2018/6/17	Very high	Very high	Very high	Very high
Luanshikeng landslide	43547	2018/6/16	Very high	High	Very high	Very high
Accuracy			0.895	0.789	0.895	0.789

each slope unit-based conditioning factor. In this case, more heterogeneous features of slope unit-based conditioning factors can be characterized to obtain more realistic and accurate LSP results.

7. Concluding remarks

In this study, the slope units in Chongyi County of China are extracted by the MSS method. Then the heterogeneity of the slope unit-based conditioning factors is considered to construct variant Slope-machine learning models. Fifteen grid unit-based and 22 slope unit-based conditioning factors are acquired to predict the LSIs using RF (variant Slope-RF, Slope-RF and Grid-RF) and MLP (variant Slope-MLP, Slope-MLP and Grid-MLP) models. The comparisons of AUC values and FR accuracy indicate that the LSP performances of the variant Slope-RF/MLP models are better than those of the Slope-RF/MLP models. Moreover, we demonstrate that the slope units extracted by the MSS method are appropriate for LSP modeling, and the heterogeneous features of slope unit-based conditioning factors can be well represented by the range and STD values of conditioning factors.

In conclusion, landslide information can be explored more comprehensively by efficiently extracting slope units and considering the heterogeneity of conditioning factors within the slope units. The LSP results based on the variant Slope-machine learning models have stronger practical application than those of Grid-machine learning models.

Declaration of competing interest

The authors declare that they have no known competing financial interests or personal relationships that could have appeared to influence the work reported in this paper.

Acknowledgments

This research is funded by the Natural Science Foundation of China (Grant Nos. 41807285, 41972280 and 52179103). The first author would like to thank the China Scholarship Council for funding his research at the University of Padova, Italy.

References

Achour, Y., Pourghasemi, H.R., 2020. How do machine learning techniques help in increasing accuracy of landslide susceptibility maps? Geosci. Front. 11, 871–883.
Alcántara-Ayala, I., Sassa, K., Mikoš, M., et al., 2017. The 4th World Landslide Forum: landslide research and risk reduction for advancing the culture of living with natural hazards. Int. J. Disast. Risk Sci. 8, 498–502.
Ba, Q., Chen, Y., Deng, S., Yang, J., Li, H., 2018. A comparison of slope units and grid cells as mapping units for landslide susceptibility assessment. Earth Sci. Inform. 11, 373–388.
Breiman, L., 2001. Random forests. Mach. Learn. 45, 5–32.
Bui, D.T., Tuan, T.A., Klempe, H., Pradhan, B., Revhaug, I., 2016. Spatial prediction models for shallow landslide hazards: a comparative assessment of the efficacy of support vector machines, artificial neural networks, kernel logistic regression, and logistic model tree. Landslides 13, 361–378.
Camilo, D.C., Lombardo, L., Mai, P.M., Dou, J., Huser, R., 2017. Handling high predictor dimensionality in slope-unit-based landslide susceptibility models through LASSO-penalized generalized linear model. Environ. Model. Software 97, 145–156.
Cantarino, I., Carrion, M.A., Goerlich, F., Martinez Ibañez, V., 2018. A ROC analysis-based classification method for landslide susceptibility maps. Landslides 16, 265–282.
Catani, F., Lagomarsino, D., Segoni, S., Tofani, V., 2013. Landslide susceptibility estimation by random forests technique: sensitivity and scaling issues. Nat. Hazards Earth Syst. Sci. 13, 2815–2831.
Chang, Z., Du, Z., Zhang, F., et al., 2020. Landslide susceptibility prediction based on remote sensing images and GIS: comparisons of supervised and unsupervised machine learning models. Rem. Sens. 12, 502.
Chen, L., Zhang, W., Chen, F., Gu, D., Wang, L., Wang, Z., 2022. Probabilistic assessment of slope failure considering anisotropic spatial variability of soil properties. Geosci. Front. 13, 101371.
Chen, X., Chen, H., You, Y., Liu, J., 2015. Susceptibility assessment of debris flows using the analytic hierarchy process method – A case study in Subao river valley, China. J. Rock Mech. Geotech. Eng. 7, 404–410.
Darabi, H., Moradi, E., Davudirad, A.A., Ehteram, M., Cerda, A., Haghighi, A.T., 2021. Efficient rainwater harvesting planning using socio-environmental variables and data-driven geospatial techniques. J. Clean. Prod. 311, 127706.
Domènech, G., Alvioli, M., Corominas, J., 2019. Preparing first-time slope failures hazard maps: from pixel-based to slope unit-based. Landslides 17, 249–265.
Donnini, M., Napolitano, E., Salvati, P., Ardizzone, F., Bucci, F., Fiorucci, F., Santangelo, M., Cardinali, M., Guzzetti, F., 2017. Impact of event landslides on road networks: a statistical analysis of two Italian case studies. Landslides 14, 1521–1535.
Guzzetti, F., Carrara, A., Cardinali, M., Reichenbach, P., 1999. Landslide hazard evaluation: a review of current techniques and their application in a multi-scale study, Central Italy. Geomorphology 31, 181–216.
Guzzetti, F., Reichenbach, P., Cardinali, M., Galli, M., Ardizzone, F., 2005. Probabilistic landslide hazard assessment at the basin scale. Geomorphology 72, 272–299.
Hölbling, D., Füreder, P., Antolini, F., Cigna, F., Casagli, N., Lang, S., 2012. A semi-automated object-based approach for landslide detection validated by persistent scatterer interferometry measures and landslide inventories. Rem. Sens. 4, 1310–1336.
Hölbling, D., Friedl, B., Eisank, C., 2015. An object-based approach for semi-automated landslide change detection and attribution of changes to landslide classes in northern Taiwan. Earth Sci. Inform. 8, 327–335.
Huang, F., Cao, Z., Jiang, S.-H., Zhou, C., Huang, J., Guo, Z., 2020. Landslide susceptibility prediction based on a semi-supervised multiple-layer perceptron model. Landslides 17, 2919–2930.
Huang, F., Tao, S., Chang, Z., et al., 2021. Efficient and automatic extraction of slope units based on multi-scale segmentation method for landslide assessments. Landslides 15, 1–17.
Huang, F., Yin, K., Huang, J., Gui, L., Wang, P., 2017. Landslide susceptibility mapping based on self-organizing-map network and extreme learning machine. Eng. Geol. 223, 11–22.
Hungr, O., Leroueil, S., Picarelli, L., 2013. The Varnes classification of landslide types, an update. Landslides 11, 167–194.
Jacobs, L., Kervyn, M., Reichenbach, P., Rossi, M., Marchesini, I., Alvioli, M., Dewitte, O., 2020. Regional susceptibility assessments with heterogeneous landslide information: slope unit-vs. pixel-based approach. Geomorphology 356, 107084.
Kuriakose, S.L., Devkota, S., Rossiter, D.G., Jetten, V.G., 2009. Prediction of soil depth using environmental variables in an anthropogenic landscape, a case study in the Western Ghats of Kerala, India. Catena 79, 27–38.
Lawal, A.I., Kwon, S., 2021. Application of artificial intelligence to rock mechanics: an overview. J. Rock Mech. Geotech. Eng. 13, 248–266.
Lee, S., Pradhan, B., 2006. Landslide hazard mapping at Selangor, Malaysia using frequency ratio and logistic regression models. Landslides 4, 33–41.
Merghadi, A., Yunus, A.P., Dou, J., et al., 2020. Machine learning methods for landslide susceptibility studies: a comparative overview of algorithm performance. Earth Sci. Rev. 207, 103225.
Mukaka, M.M., 2012. A guide to appropriate use of correlation coefficient in medical research. Malawi Med. J. 24 (3), 69–71.
Moosavi, V., Talebi, A., Shirmohammadi, B., 2014. Producing a landslide inventory map using pixel-based and object-oriented approaches optimized by Taguchi method. Geomorphology 204, 646–656.
Park, S.-J., Lee, C.-W., Lee, S., Lee, M.-J., 2018. Landslide susceptibility mapping and comparison using decision tree models: a case study of Jumunjin area, Korea. Rem. Sens. 10, 1545.
Pham, B.T., Bui, D.T., Prakash, I., Dholakia, M.B., 2017. Hybrid integration of Multilayer Perceptron Neural Networks and machine learning ensembles for landslide susceptibility assessment at Himalayan area (India) using GIS. Catena 149, 52–63.
Pham, B.T., Prakash, I., Dou, J., et al., 2019. A novel hybrid approach of landslide susceptibility modelling using rotation forest ensemble and different base classifiers. Geocarto Int. 35, 1267–1292.
Pradhan, B., 2010. Remote sensing and GIS-based landslide hazard analysis and cross-validation using multivariate logistic regression model on three test areas in Malaysia. Adv. Space Res. 45, 1244–1256.
Prashad Bhatt, B., Datt Awasthi, K., Prasad Heyojoo, B., Silwal, T., Kafle, G., 2013. Using geographic information system and analytical hierarchy process in landslide hazard zonation. Appl. Ecol. Environ. Res. 1, 14–22.
Reichenbach, P., Rossi, M., Malamud, B.D., Mihir, M., Guzzetti, F., 2018. A review of statistically-based landslide susceptibility models. Earth Sci. Rev. 180, 60–91.
Saha, A., Pal, S.C., Santosh, M., et al., 2021. Modelling multi-hazard threats to cultural heritage sites and environmental sustainability: the present and future scenarios. J. Clean. Prod. 320, 128713.
Samia, J., Temme, A.J.A.M., Bregt, A.K., et al., 2018. Implementing landslide path dependency in landslide susceptibility modelling. Landslides 15, 2129–2144.
Shirzadi, A., Shahabi, H., Chapi, K., et al., 2017. A comparative study between popular statistical and machine learning methods for simulating volume of landslides. Catena 157, 213–226.
Sun, X., Chen, J., Han, X., Bao, Y., Zhan, J., Peng, W., 2019. Application of a GIS-based slope unit method for landslide susceptibility mapping along the rapidly uplifting section of the upper Jinsha River, South-Western China. Bull. Eng. Geol. Environ. 79, 533–549.

Sur, U., Singh, P., Meena, S.R., 2020. Landslide susceptibility assessment in a lesser Himalayan road corridor (India) applying fuzzy AHP technique and earth-observation data. Geomatics, Nat. Hazards Risk 11, 2176–2209.
Tang, Y., Feng, F., Guo, Z., et al., 2020. Integrating principal component analysis with statistically-based models for analysis of causal factors and landslide susceptibility mapping: a comparative study from the loess plateau area in Shanxi (China). J. Clean. Prod. 277, 124159.
Tien Bui, D., Tuan, T.A., Klempe, H., Pradhan, B., Revhaug, I., 2015. Spatial prediction models for shallow landslide hazards: a comparative assessment of the efficacy of support vector machines, artificial neural networks, kernel logistic regression, and logistic model tree. Landslides 13, 361–378.
Tsai, H.-Y., Tsai, C.-C., Chang, W.-C., 2019. Slope unit-based approach for assessing regional seismic landslide displacement for deep and shallow failure. Eng. Geol. 248, 124–139.
Tsangaratos, P., Ilia, I., Hong, H., Chen, W., Xu, C., 2017. Applying Information Theory and GIS-based quantitative methods to produce landslide susceptibility maps in Nancheng County, China. Landslides 14, 1091–1111.
Tufano, R., Formetta, G., Calcaterra, D., Devita, P., 2021. Hydrological control of soil thickness spatial variability on the initiation of rainfall-induced shallow landslides using a three-dimensional model. Landslides 18, 3367–3380.
Vakhshoori, V., Zare, M., 2018. Is the ROC curve a reliable tool to compare the validity of landslide susceptibility maps? Geomatics, Nat. Hazards Risk 9, 249–266.
Wang, F., Xu, P., Wang, C., Wang, N., Jiang, N., 2017. Application of a GIS-based slope unit method for landslide susceptibility mapping along the Longzi River, Southeastern Tibetan Plateau, China. ISPRS Int. J. Geo-Inf. 6 (6), 172.
Wang, H., Liu, G., Xu, W., Wang, G., 2005. GIS-based landslide hazard assessment: an overview. Prog. Phys. Geogr. 29, 548–567.
Xie, M., Esaki, T., Zhou, G., 2004. GIS-based probabilistic mapping of landslide hazard using a three-dimensional deterministic model. Nat. Hazards 33, 265–282.
Yang, Y., Sun, G., Zheng, H., Qi, Y., 2019. Investigation of the sequential excavation of a soil-rock-mixture slope using the numerical manifold method. Eng. Geol. 256, 93–109.
Youssef, A.M., Pourghasemi, H.R., Pourtaghi, Z.S., Al-Katheeri, M.M., 2016. Landslide susceptibility mapping using random forest, boosted regression tree, classification and regression tree, and general linear models and comparison of their performance at Wadi Tayyah Basin, Asir Region, Saudi Arabia. Landslides 13, 839–856.
Zhang, B., Zhang, L., Yang, H., Zhang, Z., Tao, J., 2016. Subsidence prediction and susceptibility zonation for collapse above goaf with thick alluvial cover: a case study of the Yongcheng coalfield, Henan Province, China. Bull. Eng. Geol. Environ. 75, 1–16.
Zhang, W., Gu, X., Tang, L., Yin, Y., Liu, D., Zhang, Y., 2022a. Application of machine learning, deep learning and optimization algorithms in geoengineering and geoscience: comprehensive review and future challenge. Gondwana Res. 109, 1–17.
Zhang, W., Li, H., Han, L., Chen, L., Wang, L., 2022b. Slope stability prediction using ensemble learning techniques: a case study in Yunyang County, Chongqing, China. J. Rock Mech. Geotech. Eng. https://doi.org/10.1016/j.jrmge.2021.12.011.
Zhang, W., Li, H., Tang, L., Gu, X., Wang, L., Wang, L., 2022c. Displacement prediction of Jiuxianping landslide using gated recurrent unit (GRU) networks. Acta Geotech 17, 1367–1382.
Zhang, W., Phoon, K.-K., 2022. Editorial for Advances and applications of deep learning and soft computing in geotechnical underground engineering. J. Rock Mech. Geotech. Eng. 1674–7755.
Zhu, H., Garg, A., Yu, X., Zhou, H.W., 2022. Editorial for Internet of Things (IoT) and Artificial Intelligence (AI) in geotechnical engineering. J. Rock Mech. Geotech. Eng. 14 (4), 1025–1027.

Faming Huang obtained his BSc degree in Geographic Information System from Taiyuan University of Technology, Taiyuan, China in 2011, and his MSc and PhD degrees in Geological Engineering from China University of Geosciences, Wuhan, China in 2013 and 2017, respectively. His research interests include (1) Failure mechanism analysis of engineering and natural hazards; (2) Landslide stability and reliability analysis; (3) Landslide susceptibility, hazard and risk mapping; (4) Machine learning and numerical simulation in geological engineering; and (5) Remote sensing and geographic information system.